current issues in molecular biology

MDPI

Article

Periodontal Macrophages Co-Expressing *NFATC1* and *OSCAR* Exhibit Enhanced Osteoclastogenic Transcriptional Signatures

Longping Li [1,2,3], Yang Xiao [1,2,3], Genyu Liu [1,2,3], Zhengjie Wu [1,2,3], Yiqian Hu [1,2,3] and Qilin Li [1,2,3,*]

[1] Department of Stomatology, Tongji Hospital, Tongji Medical College, Huazhong University of Science and Technology, Wuhan 430030, China; u202314020@hust.edu.cn (L.L.)
[2] School of Stomatology, Tongji Medical College, Huazhong University of Science and Technology, Wuhan 430030, China
[3] Hubei Province Key Laboratory of Oral and Maxillofacial Development and Regeneration, Wuhan 430022, China
* Correspondence: qilinli@tjh.tjmu.edu.cn

Abstract

Background: The transcriptional features linking periodontal macrophages to osteoclast-associated processes remain incompletely characterized. We investigated whether co-expression of osteoclast-associated receptor (OSCAR) and nuclear factor of activated T cells 1 (NFATC1) identifies an osteoclast-associated macrophage state. **Methods**: Public genetic and bulk transcriptomic resources were used for exploratory candidate screening, followed by single-cell analysis of periodontal tissues from four healthy controls and five patients with periodontitis. Macrophages were characterized using regulatory network inference, virtual NFATC1 perturbation, pseudotime analysis and osteoclast-associated gene-set scoring. **Results**: OSCAR expression was enriched in macrophages, which also showed relatively high inferred NFATC1-associated activity. Macrophages co-expressing NFATC1 and OSCAR had higher osteoclast-associated signature scores than other macrophages. Also, their proportion showed a modest increase in periodontitis. IRF7-high macrophages expressed more IRF8 and less NFATC1 and OSCAR than osteoclast-associated macrophages. The inferred ordering of these states showed declining IRF8 expression and a modest late increase in OSCAR. Virtual NFATC1 perturbation highlighted network changes involving immune and osteoclast-related processes. **Conclusions**: NFATC1 and OSCAR co-expression marks a candidate osteoclast-associated transcriptional state in periodontal macrophages. These findings help characterize periodontal macrophage heterogeneity and identify a cell state for further investigation of inflammatory bone loss. Functional validation is needed to determine its capacity for osteoclast differentiation and bone resorption.

Keywords: periodontitis; macrophages; OSCAR; NFATC1; single-cell RNA sequencing; osteoclastogenesis

Academic Editors: Alessandro Polizzi and Gaetano Isola

Received: 24 October 2026
Revised: 16 November 2026
Accepted: 19 November 2026
Published: 23 November 2026

Copyright: © 2026 by the authors. Licensee MDPI, Basel, Switzerland. This article is an open access article distributed under the terms and conditions of the Creative Commons Attribution (CC BY) license.

1. Background

Periodontitis is a chronic inflammatory disease associated with dysbiotic dental biofilms and a dysregulated host response. Progressive destruction of the periodontal supporting tissues can lead to periodontal pocket formation, attachment loss, alveolar bone

resorption and tooth loss [1,2]. Its prevalence and associations with systemic disorders make it an important oral and general health problem [3,4].

Alveolar bone loss reflects an imbalance between bone resorption and formation in the inflamed periodontal microenvironment. Immune–stromal interactions can increase receptor activator of nuclear factor-kappa B ligand (RANKL) expression and promote osteoclastogenesis [5,6]. Macrophages participate in inflammatory responses and belong to the myeloid lineage from which osteoclast precursors arise [7,8]. However, expression of osteoclast-associated genes in a macrophage does not establish the identity or function of a mature, multinucleated osteoclast. Distinguishing inflammatory activation from osteoclast-associated transcriptional states is therefore important when interpreting periodontal myeloid heterogeneity.

RANKL–RANK signaling cooperates with costimulatory pathways to support osteoclast differentiation [9–11]. OSCAR is an immunoglobulin-like receptor involved in these pathways and has also been investigated in osteoarthritis [10,12,13]. NFATC1 integrates RANKL-dependent and calcium-dependent differentiation signals [14]. NFATC1-induced OSCAR transcription during osteoclastogenesis was demonstrated previously [15]; the regulatory relationship itself is therefore established. The question addressed here is how NFATC1-associated activity and OSCAR expression are distributed across macrophage states in human periodontal tissue.

We focused on three questions: which periodontal cell populations express OSCAR; how OSCAR expression relates to inferred NFATC1 activity; and whether macrophages coexpressing NFATC1 and OSCAR display stronger osteoclast-associated transcriptional signatures than other macrophages. These questions concern cellular associations and candidate states, rather than direct demonstration of a causal pathway from genetic variation to alveolar bone loss.

We examined public genetic and bulk transcriptomic resources together with a human periodontal single-cell dataset. Regulatory network inference, gene-set scoring, virtual perturbation and pseudotime analysis were used to characterize NFATC1/OSCAR-associated macrophage states. The study provides hypotheses for functional investigation of periodontal osteoimmunology.

2. Methods

2.1. Data Sources

Genetic datasets included FinnGen summary statistics for chronic periodontitis, OSCAR-related genetic association data, and cis-eQTL resources: GTEx_Analysis_v10_eQTL and QTS000046. Genetic dataset characteristics are summarized in Supplementary Table S1 (Genome build: GRCh38(hg38)). These resources were used for exploratory genetic candidate screening and regional comparison of association signals.

Bulk transcriptomic data were obtained from GEO: GSE79705 [16] and GSE316444 [17]. GSE79705 is a human gingival microarray dataset with healthy controls, individuals with a history of chronic periodontitis (CP), and individuals with a history of generalized aggressive periodontitis (GAgP). We included the four CP samples (GSM2101361–GSM2101364) and four healthy controls (GSM2101365–GSM2101368); the four GAgP samples were excluded. The sampled gingiva were clinically healthy tissue from edentulous sites, including in participants with a history of periodontitis. GSE316444 derives from a mouse study of ligature-induced periodontitis and traumatic occlusion. Four control and four periodontitis samples were selected for the present bulk analysis. The two datasets differ in species, platform and sampling context.

Human single-cell RNA sequencing data were obtained from GSE171213 [18]. We analyzed nine untreated periodontal tissue samples: four healthy controls (HC1–HC4; GSM5220920–GSM5220923) and five periodontitis samples (PD1–PD5; GSM5220924–

GSM5220928). The three post-treatment samples (PDT1–PDT3; GSM5220929–GSM5220931) were excluded from this comparison.

Gene Ontology (GO) and Kyoto Encyclopedia of Genes and Genomes (KEGG) annotations were used for gene-set enrichment. Transcription factor annotations supported candidate selection. SCENIC with AUCell, scTenifoldKnk and Slingshot were used for regulatory network inference, virtual perturbation and pseudotime analysis, respectively [19–21].

2.2. Analytical Methods

2.2.1. Bulk Transcriptomic Processing and Differential-Expression Screening

The bulk workflow used log2 transformation, global quantile normalization and ComBat batch adjustment. Sample expression distributions were examined using box plots. Orthologous gene mapping between human and mouse was performed using the Mouse Genome Informatics (MGI) orthology database. Only one-to-one ortholog pairs were retained for downstream integrated analysis; genes with ambiguous or non-one-to-one orthology relationships were excluded to avoid mapping bias during cross-species comparison.

Differentially expressed genes (DEGs) were screened using an absolute log2 fold change greater than 0.5 and a false discovery rate (FDR)-adjusted p value below 0.05. Expression patterns were displayed using a z-score heatmap, and differential-expression results were summarized in a volcano plot.

GO and KEGG enrichment analyses were applied to the DEG set. Single-sample gene set enrichment analysis (ssGSEA) was used to calculate cell-type-associated signature scores in bulk samples. These scores represent relative transcriptional enrichment and were not interpreted as measured cell proportions.

2.2.2. Exploratory Genetic Analysis of OSCAR-Associated Signals

OSCAR-related genetic association results were summarized in a Manhattan plot. Regional GWAS and cis-eQTL association signals were compared to investigate candidate shared signals (lead SNP: rs10500316).

Genes associated with the candidate variants were retained for downstream overlap and enrichment analyses. Regional similarity between association signals was treated as exploratory evidence and not as proof of a causal variant or a disease mechanism.

GO and KEGG enrichment analyses were used to describe functional annotations of the candidate genes, including osteoclast-related and immune-related terms.

2.2.3. Intersection of Genetic Candidates and Transcriptomic Gene Sets

The OSCAR-associated candidate gene set was intersected with the bulk DEG set. Expression distributions of the overlapping genes were displayed using combined box and violin plots in the same bulk dataset; these plots did not constitute independent validation.

Periodontitis-associated candidate genes were obtained from the genetic screening workflow using chronic periodontitis GWAS and cis-eQTL data (lead SNP: rs9748916).

These candidate genes were intersected with the bulk DEG set and a transcription factor list. The overlap was used to nominate candidate regulators for further single-cell characterization, without assigning causality from set membership alone.

2.2.4. Single-Cell Quality Assessment and Cell Annotation

Cellular UMI counts, detected gene counts and mitochondrial transcript percentages were examined for quality assessment. The analysis selected 3000 highly variable genes and the first 12 principal components based on the elbow plot. Seurat integration was used to reduce sample-associated technical variation.

Uniform manifold approximation and projection (UMAP) was used for visualization. Clusters were annotated using marker gene expression, and dot plots were used to examine OSCAR and NFATC1 across the annotated populations.

Ligand–receptor analysis was used to infer potential interactions among immune and stromal populations. These predictions describe transcript-compatible communication candidates rather than directly measured signaling.

2.2.5. NFATC1-Associated Regulatory Activity and Pseudotime Inference

SCENIC and AUCell were used to examine an NFATC1-associated transcriptional module [19]. The module reported in the analysis included TNF, IL2, IL6, CSF1R and AIF1. AUCell scores summarized the relative enrichment of module genes in individual cells. Motif-supported or coexpression-based assignments were interpreted as regulatory predictions rather than experimentally confirmed direct targets.

Pseudotime analysis was used to order transcriptionally related macrophage states. Expression trends of NFATC1 and OSCAR were examined across the inferred ordering. Spearman correlation was used to describe the relationship between OSCAR expression and the NFATC1-associated AUCell score.

2.2.6. Virtual NFATC1 Perturbation in Macrophages

scTenifoldKnk was used to perturb NFATC1 in an inferred macrophage gene regulatory network [20]. The method compares perturbed and unperturbed networks to identify genes with altered regulatory relationships.

Network perturbation scores and associated significance measures were used to characterize affected genes. The standardized perturbation scores were not interpreted as measured expression fold changes.

GO and KEGG annotations were examined for genes identified by the virtual perturbation analysis.

The resulting annotations were used to identify processes potentially connected to NFATC1-associated network organization. Enrichment alone does not establish pathway activation or inhibition, and the virtual perturbation does not substitute for experimental gene deletion.

2.2.7. NFATC1 and OSCAR Coexpression and Osteoclast-Associated Signature Scoring

Cells with normalized expression > 0 for both NFATC1 and OSCAR (RNA assay, data layer in Seurat4.3.0) were defined as $NFATC1^{+}OSCAR^{+}$ double-positive macrophages. This operational definition refers to RNA detection and does not establish protein coexpression. Their positions were displayed on the UMAP embedding.

Macrophages were reclustered and annotated using marker profiles. Nine descriptive states were reported, including M1-like, M2-like, osteoclast-associated and IRF7-high macrophages. Labels were used to summarize transcriptional features rather than establish discrete functional lineages.

For each sample, the double-positive proportion was calculated using the number of double-positive macrophages divided by the total macrophage count. Sample-level distributions in healthy controls and periodontitis were compared descriptively.

ssGSEA was used to summarize an osteoclast-associated gene set (CSF1, CSF1R, TNFSF11, TNFRSF11A, DCSTAMP, ITGB3) in double-positive and other macrophages

and across annotated macrophage states. Scores were interpreted as transcriptional signatures, rather than measurements of osteoclast differentiation or bone resorption.

2.2.8. Comparison and Pseudotime Ordering of Macrophage States

IRF7-high and osteoclast-associated macrophages were compared using differential-expression screening with an absolute log2 fold change greater than 0.5 and adjusted p below 0.05. Results were summarized in a volcano plot.

Expression distributions of IRF7, IRF8, NFATC1 and OSCAR were displayed for the two macrophage states.

GO enrichment analyses were performed separately for the gene sets associated with each state.

Slingshot was used to infer an ordering from the IRF7-high state toward the osteoclast-associated state [21]. This orientation was an analytical choice. Expression trends were examined along the resulting pseudotime, which was not interpreted as elapsed time or evidence of lineage conversion.

2.3. Use of AI Tools

OpenAI Codex was used to assist with language editing and manuscript organization. It was not used to generate or reanalyze the research data. The authors are responsible for the scientific content and final wording.

2.4. Ues of Software Tools

Software analysis and visualization were performed using R (version 4.2.3) with RStudio (2024.12.0.0) as the integrated development environment for high-throughput data processing, bioinformatic analyses and custom statistical plotting. GraphPad Prism (version 9.0.0) was used for conventional statistical analysis and visualization of wet experimental data. The mechanistic schematic in Figure 8 was generated using BioRender (https://BioRender.com).

3. Results

3.1. Bulk Differential-Expression and Cell-Type Signature Analysis

The bulk workflow combined GSE79705 and GSE316444 and summarized sample expression distributions before and after processing (Figure 1A). It yielded 2227 DEGs, comprising 1165 upregulated and 1062 downregulated genes (Figure 1B,C). GO terms included nuclear division, cytokine production, ossification and leukocyte migration (Figure 1D). The pathway display included cytokine–cytokine receptor interaction, cell cycle, Rap1, Wnt, integrin-related and extracellular-matrix-related annotations (Figure 1E). Not all displayed terms met the same adjusted significance threshold, so the plots were interpreted as ranked enrichment summaries. Bulk ssGSEA scores differed for selected cell-type signatures, including M1-like macrophages (Figure 1F). These are results of the combined bulk workflow and cannot by themselves establish changes within human periodontal lesions, given the species and sampling differences between its inputs.

3.2. Exploratory OSCAR-Associated Genetic and Transcriptomic Candidates

The OSCAR-related genetic analysis displayed a prominent chromosome 19 association signal and additional signals on other chromosomes (Figure 2A). Regional GWAS and cis-eQTL plots were examined for candidate shared signals (Figure 2B). Genes assigned to the candidate set were associated with osteoclast differentiation in the KEGG summary and granule-related and immune-receptor-related terms in the GO summary (Figure 2C,D). The displayed GO terms include cellular-component and molecular-

function annotations; they are not exclusively biological processes. These results nominate candidate annotations and do not establish a shared causal variant or functional mechanism.

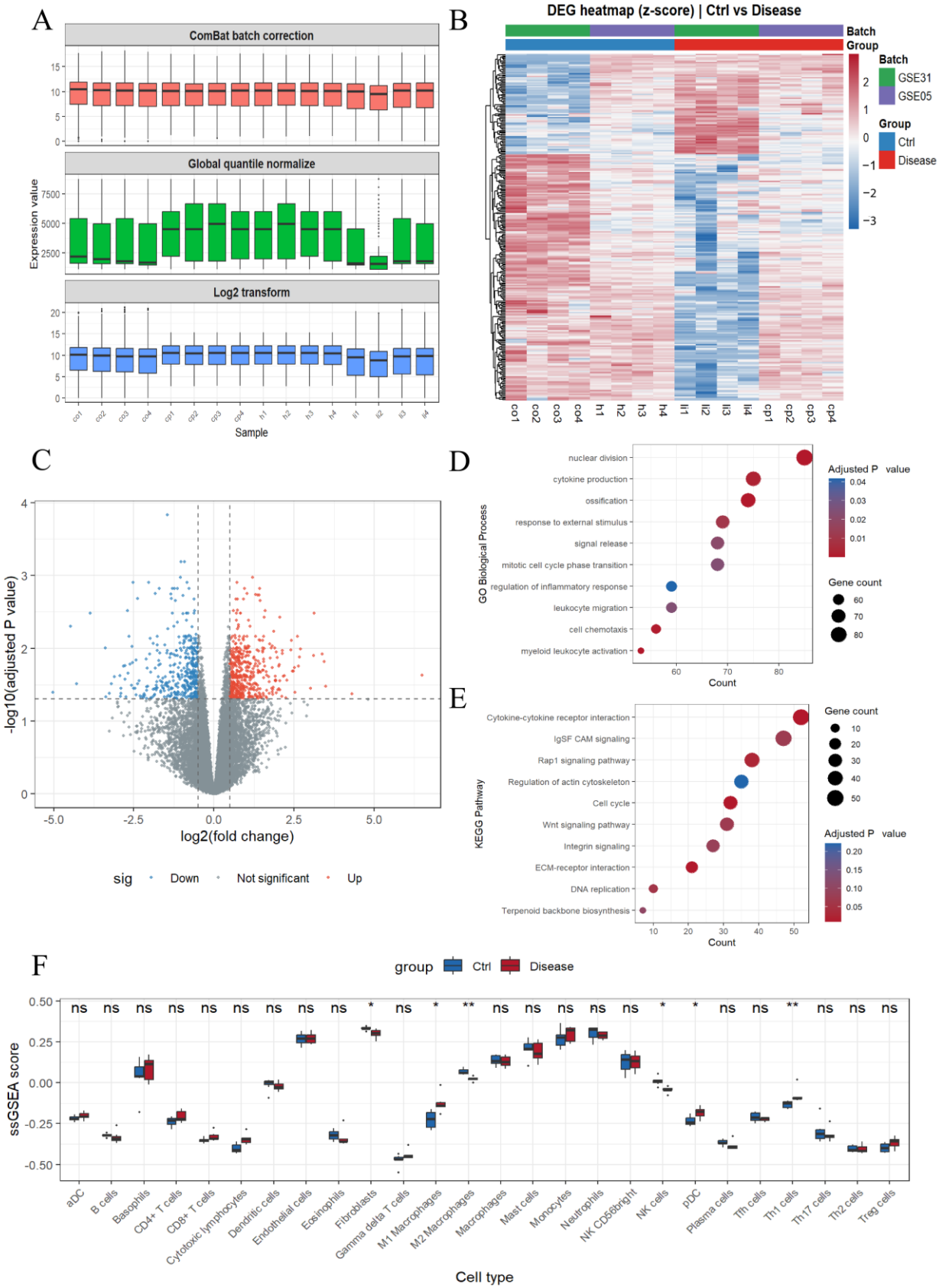

https://doi.org/10.3390/cimb48121279

Figure 1. Bulk transcriptomic processing and enrichment summaries. (**A**) Expression distributions at the processing stages displayed in the figure. (**B**) Z-score heatmap of the bulk DEG set. (**C**) Volcano plot of differential-expression results. (**D**) GO enrichment summary. (**E**) Pathway enrichment summary. (**F**) Bulk ssGSEA cell-type signature scores in the groups labeled control and disease. Signature scores are relative enrichment measures, not cell fractions. ns, not significant; * $p < 0.05$; ** $p < 0.01$. The bulk input datasets differ in species and sampling context.

Intersecting the OSCAR-associated candidate set with the bulk DEGs identified NDUFA3, OSCAR and TMC4 (Figure 2E). Within the same bulk expression dataset, NDUFA3 and OSCAR were higher, and TMC4 was lower in the group labeled disease (Figure 2F). This visualization describes the screening dataset rather than an independent validation cohort.

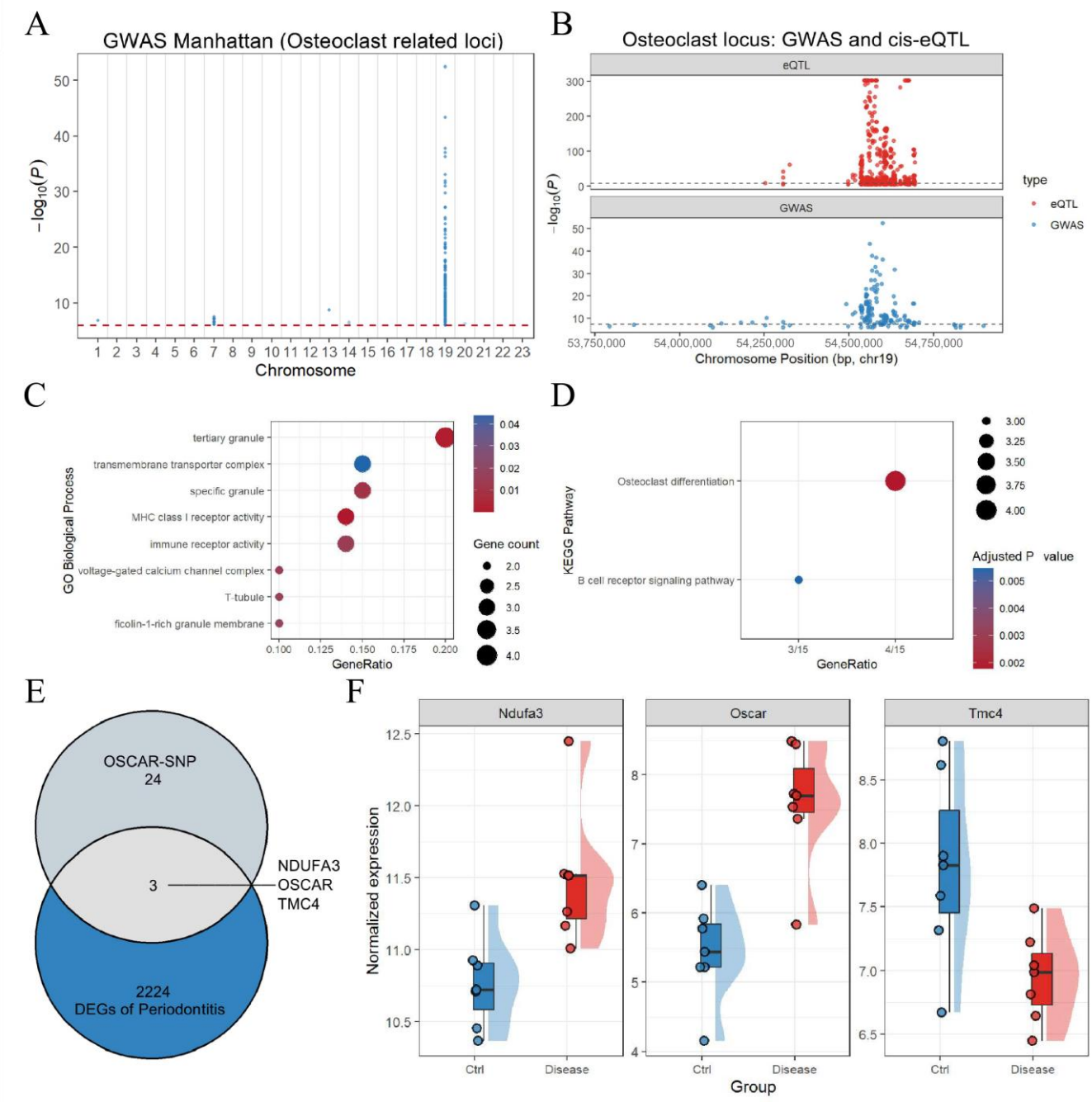

Figure 2. Exploratory genetic signals and overlapping transcriptomic candidates. (**A**) Manhattan plot from the OSCAR-related genetic workflow. Red dashed line: the GWAS whole-genome

significance threshold (typically $P = 5 \times 10^{-8}$, corresponding to $-\log_{10}(P) = 6$). (**B**) Regional GWAS and cis-eQTL association plots. (**C**) GO annotation summary for the candidate genes. (**D**) KEGG enrichment summary. Bubble size indicates gene count and color indicates adjusted *p* value. (**E**) Overlap between the OSCAR-associated candidate set and bulk DEGs. (**F**) Expression distributions of NDUFA3, OSCAR and TMC4 in the same bulk dataset. Blue represents the control group and red represents the disease group.Regional association plots alone do not establish colocalization.

3.3. Nomination of NFATC1 Through Intersecting Candidate Gene Sets

Periodontitis GWAS results and regional cis-eQTL signals were examined in the genetic screening workflow (Figure 3A,B). Intersecting the resulting candidate list, the bulk DEG set, and transcription factor annotations yielded NFATC1 as the sole three-way overlap (Figure 3C). A candidate regulatory network linked NFATC1 to OSCAR and immune-related genes, including IL4, IL2, FOXP3 and CSF2 (Figure 3D). These predictions motivated the subsequent single-cell analyses. Set overlap and database-derived regulatory edges do not establish that NFATC1 directly regulates OSCAR in the sampled periodontal cells.

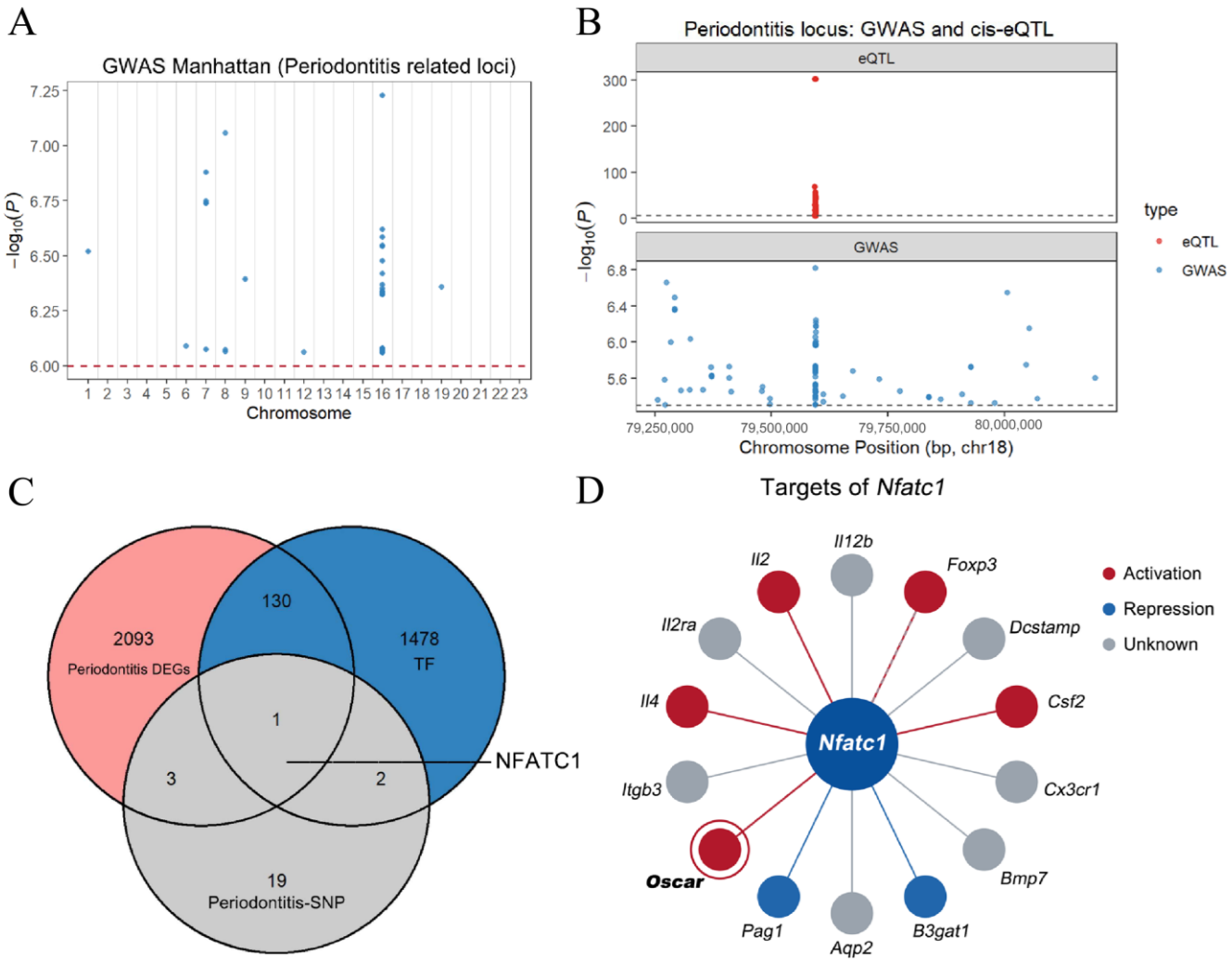

Figure 3. Candidate NFATC1 selection and regulatory relationships. (**A**) Manhattan plot from the periodontitis genetic analysis. The red dashed line represents the suggestive GWAS significance threshold, with a value of ($-\log_{10}(P) = 6.00$. (**B**) Regional association display used in candidate screening. (**C**) Intersection of periodontitis candidate genes, bulk DEGs and transcription factors. (**D**) Candidate NFATC1 regulatory relationships, with activation, repression or unknown direction

as annotated in the source network. The network provides hypotheses rather than experimentally established regulation in periodontal macrophages.

3.4. Periodontal Single-Cell Atlas and Virtual NFATC1 Perturbation

Nine human periodontal tissue samples were used for single-cell analysis. Quality metrics, highly variable gene selection, the principal-component elbow plot, sample distribution on UMAP and marker expression are shown in Figure S1. The analysis selected 3000 highly variable genes and 12 principal components. Sample mixing on the integrated embedding was used to assess integration but does not establish the absence of technical bias.

The analysis resolved 21 clusters, subsequently grouped into major cell populations using marker expression. These included T cells, B cells, plasma cells, neutrophils, endothelial cells, mast cells, fibroblasts, epithelial cells and macrophages (Figures 4A and S1E). OSCAR expression was enriched in macrophages. NFATC1 transcript abundance was highest in mast cells, with lower expression in other populations (Figure 4B). Transcript abundance alone does not establish the principal site of NFATC1 protein activity.

Ligand–receptor analysis predicted interactions among immune and stromal populations (Figure 4C,D). T cells had numerous predicted connections, while macrophages showed potential interactions with several other populations. These networks provide a transcriptional context for intercellular communication hypotheses.

Virtual NFATC1 perturbation identified genes with altered inferred regulatory relationships in macrophages (Figure 4E). GO annotations included cytokine regulation, chemotaxis, phagocytosis, endocytosis and bone-related processes (Figure 4F). The pathway display included phagocytosis, lysosomal functions, osteoclast differentiation, efferocytosis and MAPK-related annotations (Figure 4G). Enrichment significance varied across the displayed terms.

The scTenifoldKnk output describes network sensitivity to an in silico NFATC1 perturbation. A positive standardized perturbation score does not by itself indicate expression upregulation, and the analysis does not establish that NFATC1 is a negative regulator of osteoclastogenesis.

Together, these observations place OSCAR expression and NFATC1-associated network features within the macrophage compartment. They support further investigation of the established NFATC1–OSCAR relationship in periodontal tissue, without demonstrating a direct regulatory mechanism or bone-resorbing function in these cells.

3.5. Bulk Signature Associations and Single-Cell NFATC1-Associated Activity

In the bulk dataset, we examined NFATC1 and OSCAR expression against the M1 macrophage-associated ssGSEA score separately in the groups labeled control and disease (Figure 5A,B). The fitted trends differed descriptively between groups. The small sample size and broad uncertainty do not establish a difference between correlation coefficients, M1-independent induction or autonomous activation of an NFATC1–OSCAR pathway. These bulk sample-level plots are separate from the single-cell analyses in Figure 5C–F.

Single-cell SCENIC/AUCell analysis showed relatively high NFATC1-associated module scores in macrophages (Figure 5C). This distribution differed from the NFATC1 transcript pattern in Figure 4B, illustrating that transcript abundance and inferred gene-set activity need not coincide. Neither measurement directly establishes NFATC1 protein activation or promoter occupancy.

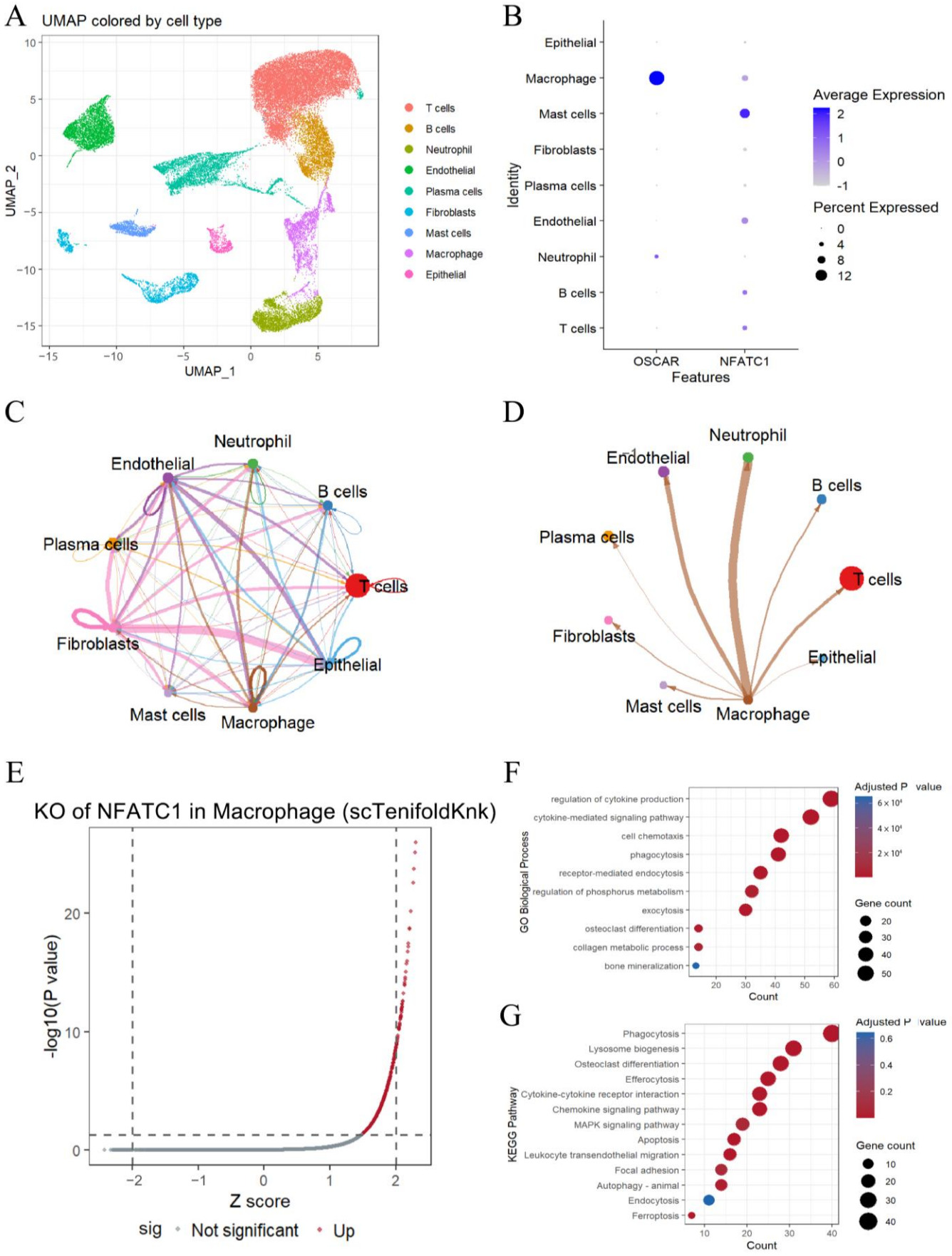

Figure 4. Periodontal cell populations and virtual NFATC1 network perturbation. (**A**) UMAP of annotated major populations. (**B**) OSCAR and NFATC1 transcript expression across populations. (**C**) Global predicted ligand–receptor network. (**D**) Macrophage-centered predicted network. (**E**)

Standardized scTenifoldKnk perturbation scores and associated significance measures. Gray dots represent non-significant genes, and red dots represent significantly upregulated genes. (**F**) GO annotation summary for affected genes. (**G**) Pathway enrichment summary in the lower enrichment panel. Network perturbation scores do not measure expression fold changes; displayed enrichment does not establish pathway activation.

The inferred trajectory described variation in macrophage transcriptional states (Figure 5D). In this ordering, OSCAR expression declined and subsequently rose, while NFATC1 showed a more modest fitted increase (Figure 5E). OSCAR expression correlated with the NFATC1-associated AUCell score at the cell level (Spearman's rho = 0.366; Figure 5F). OSCAR was included in the reported module, so the association is partly non-independent. Cells were nested within nine tissue samples, and the cell-level correlation does not constitute donor-level replication.

These results describe co-occurring transcriptional features in macrophages. They are compatible with the previously established NFATC1–OSCAR relationship but do not independently confirm regulatory direction in periodontal tissue.

3.6. NFATC1 and OSCAR Coexpressing Macrophages and Transcriptional Signatures

Macrophages with detectable NFATC1 and OSCAR transcripts were identified and displayed on the UMAP embedding (Figure 6A). These cells were a minority within the macrophage compartment; the embedding alone does not establish a distinct subcluster. Marker expression across macrophage clusters is summarized in Figure 6B. Although double-positive proportions varied among the nine samples and some were below 1%, the number of double-positive cells in the disease group was approximately three-fold higher than that in control samples (Figures 6C and S2A, Table S2).

Macrophage marker profiles were summarized using nine descriptive states: endocytic, M2-like, resident-like, NLRP3-positive, MHC-II-high, IRF7-high, proliferative, M1-like and osteoclast-associated macrophages (Figures 6D and S2B). Double-positive cells had higher osteoclast-associated ssGSEA scores than the remaining macrophages (Figures 6E and S2C,D). Meanwhile, the osteoclast-associated ssGSEA scores of double-positive cells in the disease group were also higher than those in the control group (Figure S2E). The state labeled osteoclast-associated had the highest scores, whereas the IRF7-high state had lower scores (Figure 6F). These comparisons describe transcriptomic differences; their independence from the defining genes and annotation markers has not been established. They do not demonstrate osteoclast formation or bone resorption.

3.7. Expression Differences and Pseudotime Ordering of Macrophage States

IRF7-high and osteoclast-associated macrophages showed distinct expression patterns (Figure 7A,B). IRF7 and IRF8 were higher in the IRF7-high state, whereas NFATC1 and OSCAR were higher in the osteoclast-associated state. These expression comparisons used the same single-cell dataset and were not independent validation experiments.

In the NFATC1^{+}OSCAR^{+} double-positive macrophages, genes associated with the osteoclast-associated state were enriched for cytokine signaling, mononuclear cell differentiation, chemotaxis, osteoclast differentiation and bone remodeling annotations (Figure 7C). IRF7-high state annotations included cytokine regulation, immune responses, leukocyte migration, wound healing and endoplasmic-reticulum stress (Figure 7D). Differences in annotation do not establish antagonistic regulatory mechanisms.

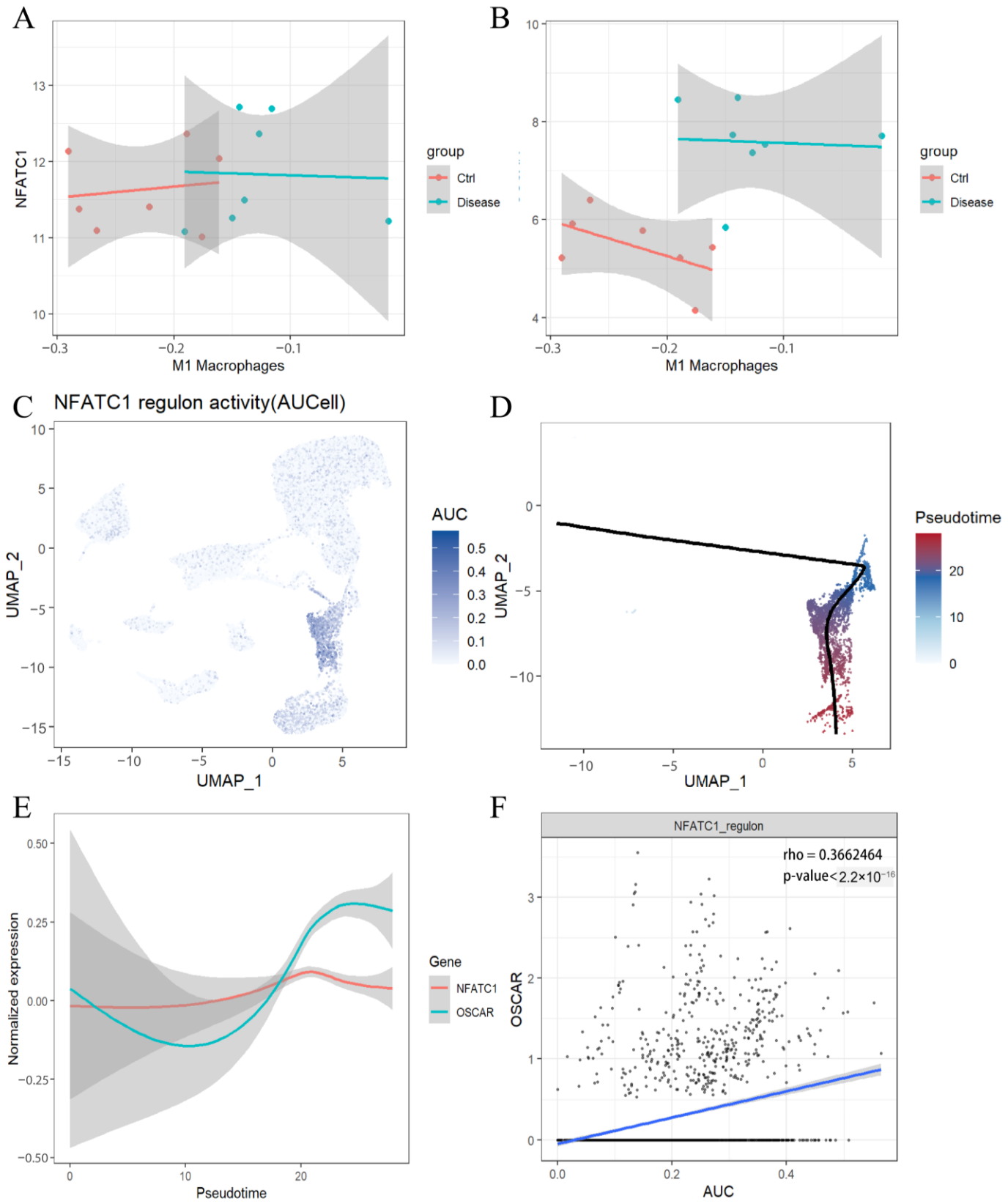

Figure 5. Bulk signature associations and inferred NFATC1-associated activity. (**A**,**B**) Bulk sample-level expression of NFATC1 and OSCAR plotted against the M1 macrophage-associated ssGSEA score in control and disease groups. The horizontal axis is a signature score, not a measured cell proportion. Panels (**C**–**F**) use single-cell data. (**C**) NFATC1-associated AUCell scores. (**D**) Inferred trajectory on the embedding. (**E**) Fitted expression trends along pseudotime. (**F**) Cell-level association between OSCAR expression and the NFATC1-associated AUCell score. The blue line

indicates the regression fit with confidence interval, and black dots correspond to individual observations. Inclusion of OSCAR in the reported module limits independence of this correlation.

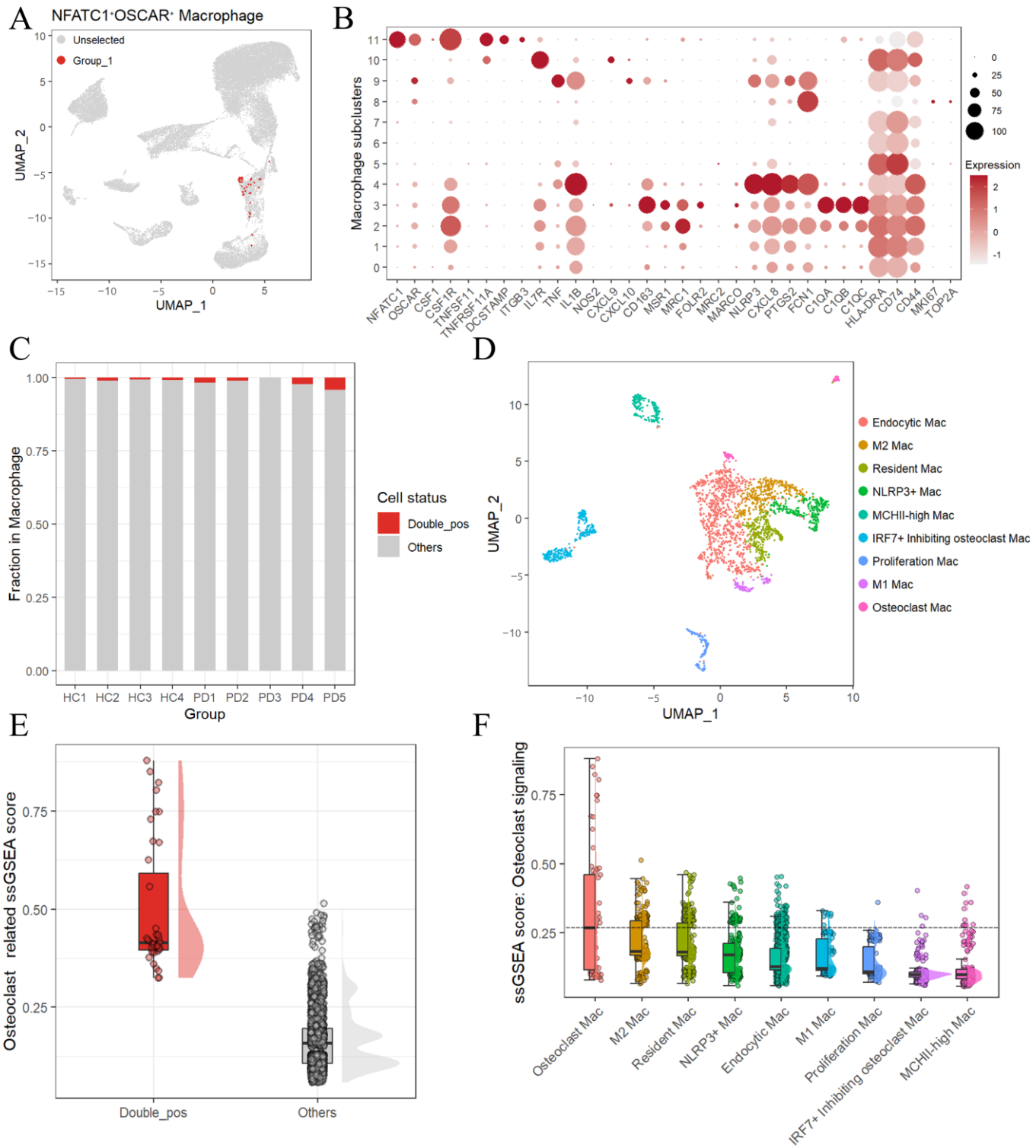

Figure 6. NFATC1 and OSCAR coexpressing macrophages and signature scores. (**A**) Cells with detectable NFATC1 and OSCAR transcripts on the UMAP embedding. (**B**) Marker expression across macrophage clusters. (**C**) Double-positive fractions within each sample's macrophage population. (**D**) Nine marker-based macrophage states. (**E**) Osteoclast-associated ssGSEA scores in double-positive and other macrophages. Red represents the NFATC1+OSCAR+ double-positive macrophages, and gray represents the others macrophages. (**F**) Scores across the annotated states. The original labels "Osteoclast Mac" and "IRF7+ Inhibiting osteoclast Mac" are interpreted here as

osteoclast-associated and IRF7-high macrophages, respectively. These are descriptive annotations, not experimentally established functions.

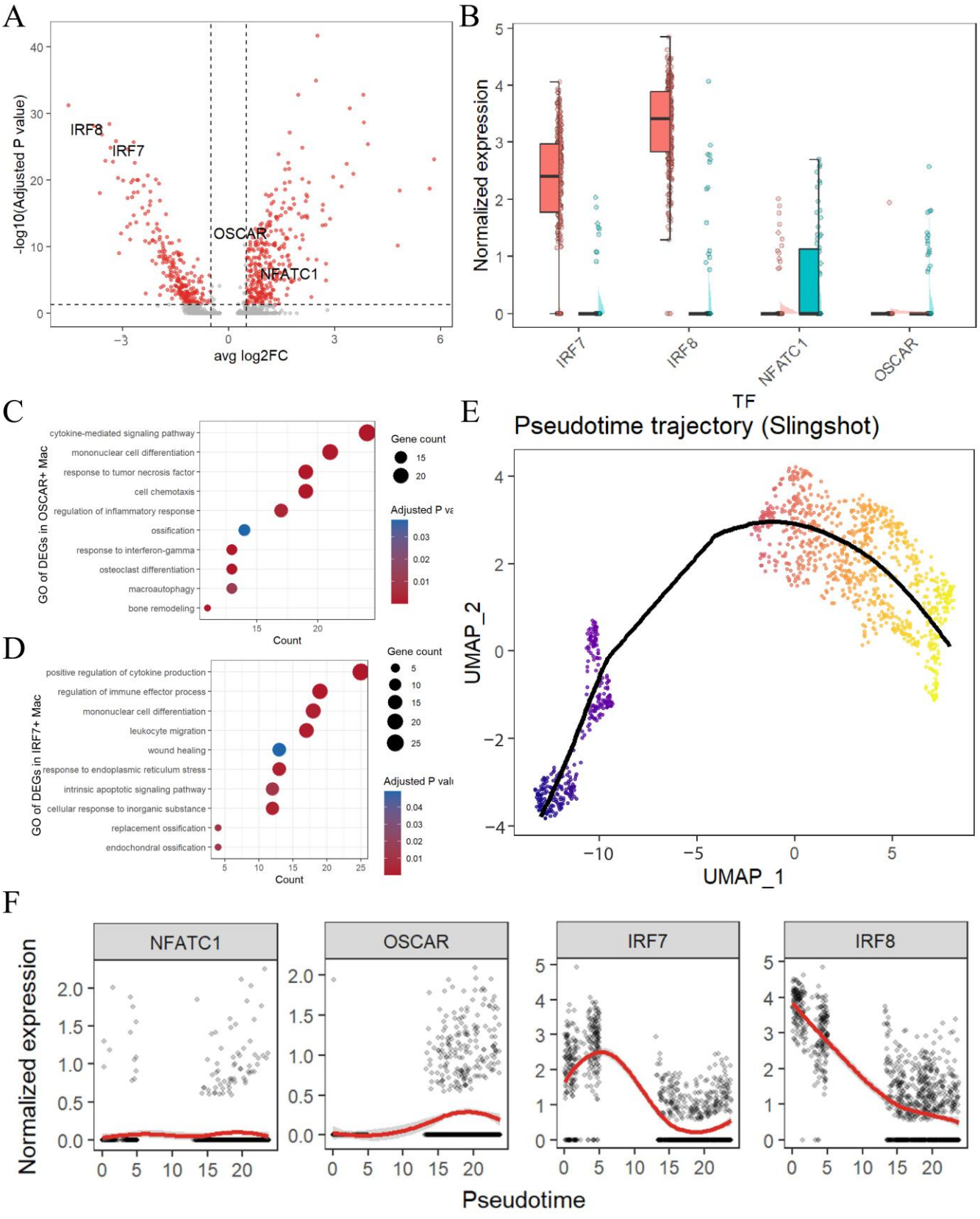

Figure 7. Expression profiles and inferred ordering of selected macrophage states. (**A**) Differential-expression display comparing IRF7-high and osteoclast-associated macrophages. Red dots denote genes with significant differential expression, gray dots denote non-significant genes. (**B**) Expression

https://doi.org/10.3390/cimb48121279

distributions of IRF7, IRF8, NFATC1 and OSCAR. Red boxes and dots represent IRF7$^+$ inhibiting osteoclast macrophages; cyan boxes and dots represent osteoclastic macrophages. (**C**) GO summaries for genes associated with NFATC1$^+$OSCAR$^+$ double-positive macrophages. (**D**) GO summaries for genes associated with IRF7-high states. (**E**) Slingshot trajectory, oriented from the IRF7-high state. The gradient color from purple through orange to yellow indicates the progression of pseudotime. The black curve shows the cell trajectory inferred by Slingshot. (**F**) Fitted gene expression across pseudotime. Pseudotime is a model-based ordering of cross-sectional profiles and does not demonstrate lineage conversion. Gray diamonds represent individual cells, and the red fitted curve depicts the dynamic expression trend of each gene along pseudotime.

Slingshot ordered the selected cells from the IRF7-high state toward the osteoclast-associated state (Figure 7E). IRF7 showed an early increase followed by a decline, and IRF8 decreased across the ordering. OSCAR showed a modest late increase, whereas the fitted NFATC1 trend remained relatively low and nearly flat in this trajectory (Figure 7F). The inferred ordering is consistent with transcriptional heterogeneity, but it does not establish a temporal switch, loss of an inhibitory mechanism or conversion of macrophages into osteoclasts.

4. Discussion

Inflammatory alveolar bone loss involves interactions between local immune responses and osteoclast differentiation [1]. Related osteoclastogenic pathways have also been investigated in apical periodontitis, although that disease context differs from marginal periodontitis [22]. Previous studies have established that OSCAR-mediated costimulation supports calcium-dependent NFATC1 signaling and that NFATC1 can induce OSCAR transcription during osteoclastogenesis [10,15,23]. Our study examines the cellular distribution of these established relationships in periodontal transcriptomic data.

The main observation is that NFATC1-and-OSCAR-co-expressing macrophages showed higher osteoclast-associated signature scores than the remaining macrophages. OSCAR expression was enriched in macrophages, and NFATC1-associated AUCell activity differed from the distribution of NFATC1 transcripts. These findings identify a candidate transcriptional state for further study. They do not establish a previously unknown regulatory axis or show that the identified macrophages cause alveolar bone loss.

The genetic and bulk analyses were used for exploratory candidate nomination. Their interpretation requires particular caution. GSE79705 samples came from clinically healthy gingiva in people with or without a history of periodontitis, whereas GSE316444 came from an experimental mouse study. Matching control and disease sample counts does not make these sampling contexts equivalent. Platform normalization and ComBat adjustment alone cannot resolve species differences. Regional GWAS/eQTL plots and gene-set overlap also do not demonstrate that a variant is causal or that genetic effects are mediated through NFATC1 and OSCAR in periodontal macrophages.

The difference between NFATC1 transcript abundance and its inferred module score is compatible with cell-type-specific regulatory contexts, but an AUCell score is a gene-set enrichment measure rather than a direct assay of transcription factor activation. Predicted ligand–receptor networks similarly suggest possible interactions rather than demonstrated signaling events.

The macrophage analysis identified contrasting IRF7/IRF8-rich and osteoclast-associated expression profiles. Pseudotime provided an ordering of these cross-sectional states, with decreasing IRF7/IRF8 expression and a modest rise in OSCAR. NFATC1 did not show the same pronounced trajectory in every analysis. These results support investigation of macrophage heterogeneity, while lineage tracing or time-resolved functional

experiments would be needed to establish a transition or an inhibitory role for IRF7-high cells.

Virtual NFATC1 perturbation highlighted immune and osteoclast-related network annotations. We note that in silico perturbation results are vulnerable to technical dropout inherent to single-cell RNA-seq data. Cross-reference against curated transcription-factor databases (TRRUST, AnimalTFDB) identified partial overlap between perturbation-altered genes and documented NFATC1 downstream targets involved in osteoclastogenesis, supporting partial biological plausibility of these predictions. Due to intrinsic resolution discrepancies between single-cell and bulk transcriptomic data, we did not replicate the full perturbation workflow on independent bulk cohorts. Such computational predictions can prioritize follow-up questions but do not establish the direction of expression changes after experimental deletion and require independent experimental validation. Reanalysis showed a modest increase in the proportion of NFATC1^{+}OSCAR^{+} macrophages in periodontitis samples. However, given the small number of donors and the rarity of this population, this result should be interpreted cautiously.

Several limitations affect interpretation. First, this was a secondary analysis of public datasets without protein-level, histological or functional validation of the co-expressing macrophages. The follow-up cell-based and in vivo animal studies to empirically compare osteoclastic bone-resorbing potential among NFATC1^{+}OSCAR^{+}, single-positive, and double-negative macrophage subsets are planned as follow-up studies but were not performed in the present revision. Second, the bulk inputs differ in species, platform and sampling context, limiting the interpretation of their combined analysis. Third, genetic candidate screening cannot establish a causal mechanism without clearly documented source traits, tissue-specific eQTL inputs, genome-build harmonization and quantitative colocalization evidence. Fourth, only nine human single-cell samples were analyzed, and cells within a donor are not independent biological replicates. The complete scoring gene set and its overlap with the genes defining double-positive cells are necessary to assess circularity; the current score comparison does not establish an independent functional phenotype. RNA dropout, clustering choices and gene-set construction may also affect the detected states. Finally, the inferred trajectories and communication networks require experimental testing before mechanistic or clinical interpretation.

The practical contribution is a descriptive framework for studying NFATC1/OSCAR-associated macrophage states in periodontal tissue. It may help prioritize cells and molecular relationships for validation, but it does not establish a selective therapeutic target or superiority to existing approaches. The schematic in Figure 8 should be read as a hypothesis rather than a demonstrated mechanism.

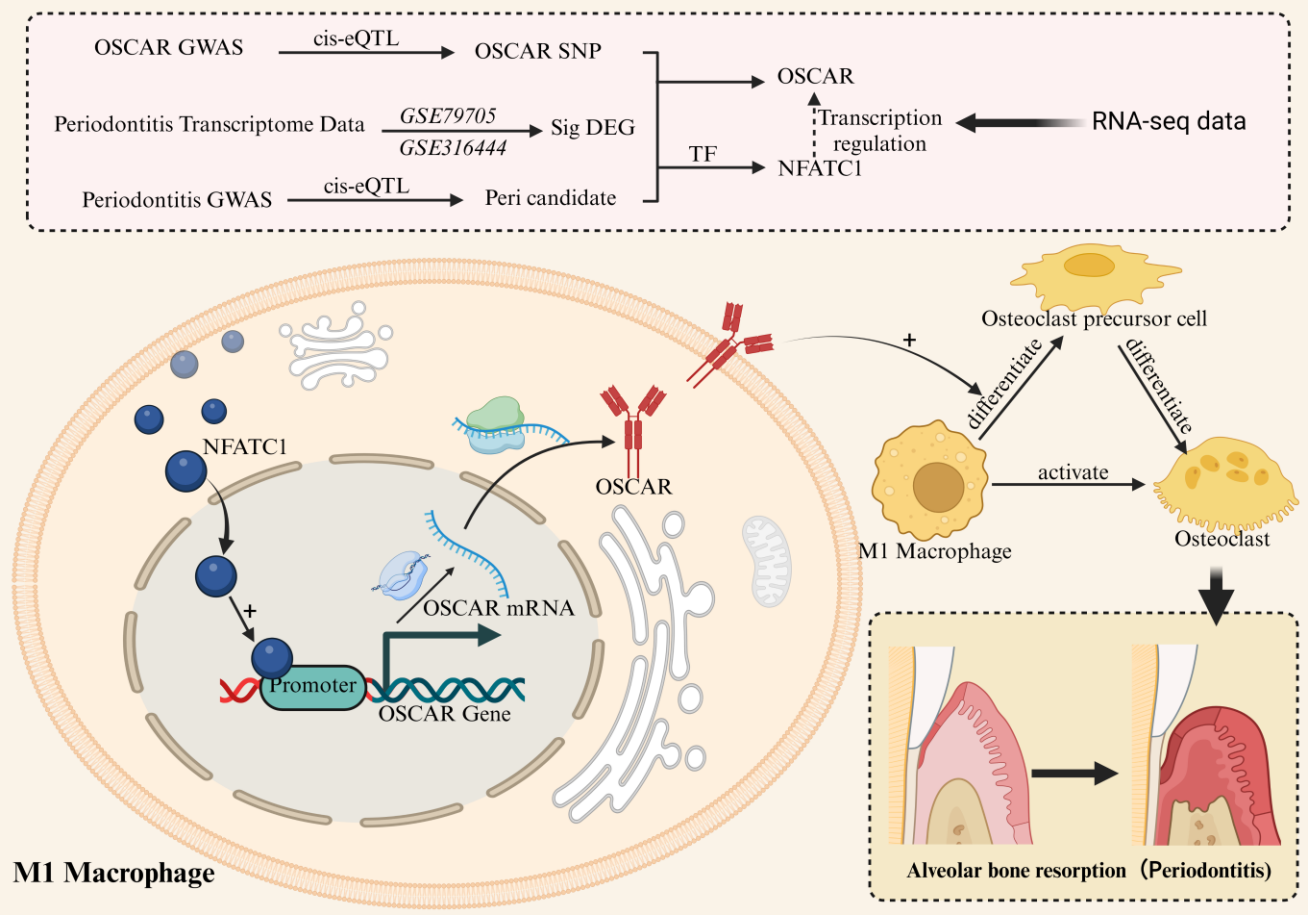

Figure 8. Proposed relationship between NFATC1 and OSCAR in periodontal macrophages. The schematic summarizes the study's candidate-selection framework and a hypothesis linking NFATC1/OSCAR-associated macrophage states with osteoclastogenesis. The regulatory direction and the connection to alveolar bone resorption are hypotheses informed by prior literature and computational observations, rather than mechanisms established by this study. Integrative genetic, bulk transcriptomic, and single-cell analyses were reported in the present analysis. Created in BioRender. Shuo Huang (2026). https://BioRender.com/7jzf266.

5. Conclusions

Macrophages co-expressing NFATC1 and OSCAR exhibited stronger osteoclast-associated transcriptional signatures in the analyzed human periodontal single-cell dataset. Analysis showed a modest increase in the proportion of NFATC1^{+}OSCAR^{+} macrophages in periodontitis samples, but its identity as a bone-resorbing effector population remains unproven. The findings provide a basis for the functional investigation of periodontal macrophage heterogeneity; direct regulation, lineage relationships and disease contribution require independent validation.

Supplementary Materials: The following supporting information can be downloaded at: https://www.mdpi.com/article/10.3390/cimb48121279/s1.

Author Contributions: Conceptualization, Q.L.; methodology, L.L.; software, L.L.; validation, L.L.; formal analysis, L.L.; investigation, L.L.; resources, Q.L.; data curation, L.L., Y.X., G.L., Z.W., Y.H.; writing—original draft preparation, L.L.; writing—review and editing, Y.X., G.L., Z.W., Y.H., Q.L.; visualization, L.L.; supervision, Q.L.; project administration, Q.L.; funding acquisition, Q.L. All authors have read and agreed to the published version of the manuscript.

Funding: This work was supported by the Natural Science Foundation of Hubei Province (Grant No. 2024AFB053), the Young Fund Cultivation Project at Tongji Hospital, Tongji Medical College, Huazhong University of Science and Technology (Grant No. 2023B16), the Open Research Fund of the State Key Laboratory of Oral & Maxillofacial Reconstruction and Regeneration (Grant No. 2025KA08).

Institutional Review Board Statement: The study was conducted in accordance with the Declaration of Helsinki. As the data were obtained from publicly accessible databases and were fully de-identified, in accordance with the Measures for Ethical Review of Life Science and Medical Research Involving Humans (2023) issued by the National Health Commission of the People's Republic of China, the research was exempted from Ethics Committee review.

Informed Consent Statement: An informed consent statement was exempted for this study, as the data were obtained from publicly accessible databases and were fully de-identified, in accordance with Measures for Ethical Review of Life Science and Medical Research Involving Humans (2023) issued by the National Health Commission of the People's Republic of China.

Data Availability Statement: The public transcriptomic datasets are available in GEO under GSE79705 (https://www.ncbi.nlm.nih.gov/geo/query/acc.cgi?acc=GSE79705), GSE316444 (https://www.ncbi.nlm.nih.gov/geo/query/acc.cgi?acc=GSE316444) and GSE171213 (https://www.ncbi.nlm.nih.gov/geo/query/acc.cgi?acc=GSE171213) [16–18]. Genetic resources were obtained from FinnGen (https://www.finngen.fi/) and GTEx (https://gtexportal.org/). Study-specific materials are available from the corresponding author upon reasonable request.

Acknowledgments: We thank Jing Wang for guidance and constructive suggestions. The original schematic in Figure 8 was prepared using BioRender (https://www.biorender.com/).

Conflicts of Interest: The authors declare that they have no competing interests.

Abbreviations

The following abbreviations are used in this manuscript:

AUCell	Area under the curve scoring of gene-set activity
CP	Chronic periodontitis
DEG	Differentially expressed gene
DP	Double-positive
eQTL	Expression quantitative trait locus
FDR	False discovery rate
GAgP	Generalized aggressive periodontitis
GEO	Gene Expression Omnibus
GO	Gene Ontology
GWAS	Genome-wide association study
HC	Healthy control
KEGG	Kyoto Encyclopedia of Genes and Genomes
NFATC1	Nuclear factor of activated T cells 1
OSCAR	Osteoclast-associated receptor
PCA	Principal component analysis
PD	Periodontitis
RANKL	Receptor activator of nuclear factor-kappa B ligand
scRNA-seq	Single-cell RNA sequencing
ssGSEA	Single-sample gene set enrichment analysis
UMAP	Uniform manifold approximation and projection
UMI	Unique molecular identifier

References

1. Molon, R.S.; Vernal, R.; Oliveira, G.E.; Steffens, J.P.; Ervolino, E.; Theodoro, L.H.; Beucken, J.J.J.P.v.D.; Tetradis, S. Inflammatory bone loss and signaling pathways in periodontitis: Mechanistic insights and emerging therapeutic strategies. *Bone Res.* **2026**, *14*, 1. https://doi.org/10.1038/s41413-025-00478-1.
2. Łasica, A.; Golec, P.; Laskus, A.; Zalewska, M.; Gędaj, M.; Popowska, M. Periodontitis: Etiology, conventional treatments, and emerging bacteriophage and predatory bacteria therapies. *Front. Microbiol.* **2024**, *15*, 1469414. https://doi.org/10.3389/fmicb.2024.1469414.
3. Ge, J.; Zhu, X.; Weng, C.; Yuan, D.; Zhao, J.; Zhao, L.; Wang, T.; Wu, Y. Periodontitis impacts on thrombotic diseases: From clinical aspect to future therapeutic approaches. *Int. J. Oral Sci.* **2024**, *16*, 58. https://doi.org/10.1038/s41368-024-00325-9.
4. Herrera, D.; Sanz, M.; Shapira, L.; Brotons, C.; Chapple, I.; Frese, T.; Graziani, F.; Hobbs, F.D.R.; Huck, O.; Hummers, E.; et al. Periodontal diseases and cardiovascular diseases, diabetes, and respiratory diseases: Summary of the consensus report by the European Federation of Periodontology and WONCA Europe. *Eur. J. Gen. Pract.* **2024**, *30*, 2320120. https://doi.org/10.1080/13814788.2024.2320120.
5. Ando, Y.; Tsukasaki, M.; Huynh, N.C.N.; Zang, S.; Yan, M.; Muro, R.; Nakamura, K.; Komagamine, M.; Komatsu, N.; Okamoto, K.; et al. The neutrophil-osteogenic cell axis promotes bone destruction in periodontitis. *Int. J. Oral Sci.* **2024**, *16*, 18. https://doi.org/10.1038/s41368-023-00275-8.
6. Ye, W.; Liao, Y.; Liu, X.; Wang, Y.; Li, T.; Zhao, Y.; He, Z.; Chen, J.; Yin, M.; Sheng, Y.; et al. Dectin-2 depletion alleviates osteoclast-induced bone loss in periodontitis via Syk/NOX2/ROS signaling. *Free Radic. Biol. Med.* **2025**, *229*, 13–29. https://doi.org/10.1016/j.freeradbiomed.2025.01.011.
7. Liu, M.; Cai, Y.; Wang, Y.; Miao, X.; Liu, X.; Wang, M.; Mao, C.; Zhao, Y.; Niu, L. Macrophages Intracellularly Gelated With Bioactive Hydrogels for Synergistic Neutralization, Eradication, and Osteopromotion in Periodontitis Treatment. *Adv. Mater.* **2026**, *38*, e19288. https://doi.org/10.1002/adma.202519288.
8. Ren, F.; Zheng, S.; Luo, H.; Yu, X.; Li, X.; Song, S.; Bu, W.; Sun, H. Fibroblast derived C3 promotes the progression of experimental periodontitis through macrophage M1 polarization and osteoclast differentiation. *Int. J. Oral Sci.* **2025**, *17*, 30. https://doi.org/10.1038/s41368-025-00361-z. Correction in *Int. J. Oral Sci.* **2025**, *17*, 53.
9. Anwar, A.; Sapra, L.; Gupta, N.; Ojha, R.P.; Verma, B.; Srivastava, R.K. Fine-tuning osteoclastogenesis: An insight into the cellular and molecular regulation of osteoclastogenesis. *J. Cell Physiol.* **2023**, *238*, 1431–1464. https://doi.org/10.1002/jcp.31036.
10. Nedeva, I.R.; Vitale, M.; Elson, A.; Hoyland, J.A.; Bella, J. Role of *OSCAR* Signaling in Osteoclastogenesis and Bone Disease. *Front Cell Dev. Biol.* **2021**, *9*, 641162. https://doi.org/10.3389/fcell.2021.641162.
11. Vitale, M.; Ligorio, C.; Richardson, S.M.; Hoyland, J.A.; Bella, J. Collagen-like Osteoclast-Associated Receptor (*OSCAR*)-Binding Motifs Show a Co-Stimulatory Effect on Osteoclastogenesis in a Peptide Hydrogel System. *Int. J. Mol. Sci.* **2023**, *25*, 445. https://doi.org/10.3390/ijms25010445.
12. Kim, J.; Ryu, G.; Seo, J.; Go, M.; Kim, G.; Yi, S.; Kim, S.; Lee, H.; Lee, J.-Y.; Kim, H.S.; et al. 5-aminosalicylic acid suppresses osteoarthritis through the *OSCAR*-PPARγ axis. *Nat. Commun.* **2024**, *15*, 1024. https://doi.org/10.1038/s41467-024-45174-6.
13. Kim, G.M.; Park, D.R.; Nguyen, T.T.H.; Kim, J.; Kim, J.; Sohn, M.H.; Lee, W.-K.; Lee, S.Y.; Shim, H. Development of Anti-*OSCAR* Antibodies for the Treatment of Osteoarthritis. *Biomedicines* **2023**, *11*, 2844. https://doi.org/10.3390/biomedicines11102844.
14. Zhu, S.; Yan, M.Q.; Masson, A.; Chen, W.; Li, Y.P. Cell signaling and transcriptional regulation of osteoclast lineage commitment, differentiation, bone resorption and diseases. *Cell Discov.* **2026**, *12*, 6. https://doi.org/10.1038/s41421-025-00853-6.
15. Kim, K.; Kim, J.H.; Lee, J.; Jin, H.M.; Lee, S.H.; Fisher, D.E.; Kook, H.; Kim, K.K.; Choi, Y.; Kim, N. Nuclear factor of activated T cells c1 induces osteoclast-associated receptor gene expression during tumor necrosis factor-related activation-induced cytokine-mediated osteoclastogenesis. *J. Biol. Chem.* **2005**, *280*, 35209–35216. https://doi.org/10.1074/jbc.M505815200.
16. Taiete, T.; Casarin, R.C.V.; Ruiz, K.G.S.; Nociti, F.H.; Sallum, E.A.; Casati, M.Z. Transcriptome of healthy gingival tissue from edentulous sites in patients with a history of generalized aggressive periodontitis. *J. Periodontol.* **2018**, *89*, 93–104. https://doi.org/10.1902/jop.2017.170221.
17. Tsuchiya, Y.; Ohsugi, Y.; Hirota, T.; Hayashi, Y.; Lin, P.; Tsukahara, Y.; Iwata, T.; Katagiri, S. Traumatic Occlusion Exacerbates Bone Resorption by Modifying Gene Expression in the Bone Tissue of Ligature-Induced Periodontitis in Mice. *J. Clin. Periodontol.* **2026**, *53*, 838–848. https://doi.org/10.1111/jcpe.70112.
18. Chen, Y.; Wang, H.; Yang, Q.; Zhao, W.; Chen, Y.; Ni, Q.; Li, W.; Shi, J.; Zhang, W.; Li, L.; et al. Single-cell RNA landscape of the osteoimmunology microenvironment in periodontitis. *Theranostics* **2022**, *12*, 1074–1096. https://doi.org/10.7150/thno.65694.

19. Aibar, S.; González-Blas, C.B.; Moerman, T.; Huynh-Thu, V.A.; Imrichova, H.; Hulselmans, G.; Rambow, F.; Marine, J.-C.; Geurts, P.; Aerts, J.; et al. SCENIC: Single-cell regulatory network inference and clustering. *Nat. Methods* **2017**, *14*, 1083–1086. https://doi.org/10.1038/nmeth.4463.
20. Osorio, D.; Zhong, Y.; Li, G.; Xu, Q.; Yang, Y.; Tian, Y.; Chapkin, R.S.; Huang, J.Z.; Cai, J.J. ScTenifoldKnk: An efficient virtual knockout tool for gene function predictions via single-cell gene regulatory network perturbation. *Patterns* **2022**, *3*, 100434. https://doi.org/10.1016/j.patter.2022.100434.
21. Street, K.; Risso, D.; Fletcher, R.B.; Das, D.; Ngai, J.; Yosef, N.; Purdom, E.; Dudoit, S. Slingshot: Cell lineage and pseudotime inference for single-cell transcriptomics. *BMC Genom.* **2018**, *19*, 477. https://doi.org/10.1186/s12864-018-4772-0.
22. Qian, Y.; Wu, J.; Yang, W.; Lyu, R.; You, Q.; Li, J.; He, Q.; Zhuang, Y.; Wang, W.; Wang, Y.; et al. FTO-associated osteoclastogenesis promotes alveolar bone resorption in apical periodontitis male rat via the HK1/USP14/RANK pathway. *Nat. Commun.* **2025**, *16*, 1519. https://doi.org/10.1038/s41467-025-56615-1.
23. Zheng, H.; Liu, Y.; Deng, Y.; Li, Y.; Liu, S.; Yang, Y.; Qiu, Y.; Li, B.; Sheng, W.; Liu, J.; et al. Recent advances of NFATc1 in rheumatoid arthritis-related bone destruction: Mechanisms and potential therapeutic targets. *Mol. Med.* **2024**, *30*, 20. https://doi.org/10.1186/s10020-024-00788-w.

Disclaimer/Publisher's Note: The statements, opinions and data contained in all publications are solely those of the individual author(s) and contributor(s) and not of MDPI and/or the editor(s). MDPI and/or the editor(s) disclaim responsibility for any injury to people or property resulting from any ideas, methods, instructions or products referred to in the content.